

## High-throughput resistivity apparatus for thin-film combinatorial libraries

K. C. Hewitt,<sup>a)</sup> P. A. Casey, and R. J. Sanderson  
*Dalhousie University, Department of Physics and Atmospheric Science, Halifax,  
 Nova Scotia B3H 3J5, Canada*

M. A. White and R. Sun  
*Dalhousie University, Department of Chemistry, Halifax, Nova Scotia B3H 4J3, Canada*

(Received 28 June 2005; accepted 18 July 2005; published online 12 September 2005)

An apparatus, capable of measuring the dc resistance versus temperature of a 49-member library prepared by thin-film deposition techniques was designed and tested. The library is deposited by dc magnetron sputtering onto 10.16 cm × 10.16 cm alumina substrates on which are placed aluminum masks consisting of 8 mm diam holes cut on a 7 × 7 grid, the center-to-center spacing being 10.15 mm. Electrical contact to the library is made in a standard van der Pauw geometry using 196 spring-loaded, gold-coated pins, four pins for each member of the library. The temperature is controlled using a helium refrigerator in combination with a liquid-nitrogen radiation shield that greatly reduces radiative heating of the sample stage. With the radiation shield, the cold finger is able to sustain a minimum temperature of 7 K and the sample stage a minimum temperature of 27 K. The temperature (27–291 K) dependent dc resistivity of a thin-film silver library of varying thickness (48–639 nm) is presented to highlight the capabilities of the apparatus. The thickness dependence of both the resistivity and the temperature coefficient of resistivity are quantitatively consistent with the literature. For thicknesses greater than about 100 nm, the room-temperature resistivity (3.4 μΩ cm) are consistent with Matthiessen's rule for 1%–2% impurity content, and the temperature coefficient of resistivity is consistent with the bulk value. For thicknesses less than 100 nm, an increase in resistivity by a factor of 8 is found, which may be due to surface and boundary scattering effects; a corresponding increase in the temperature coefficient of resistivity is consistent with a concomitant decrease in the magnitude of the elastic constants and surface scattering effects. © 2005 American Institute of Physics. [DOI: 10.1063/1.2037947]

### I. INTRODUCTION

Physical vapor deposition techniques for the production of thin-film combinatorial libraries are well established.<sup>1–6</sup> To avoid a bottleneck in analysis, one must design high-throughput physical property measurement systems. Of the many physical properties of interest, electrical transport is among the most useful as it can offer insight into band structure and collective carrier phenomena. For example, one can use temperature-dependent resistivity measurements to determine the optical band gap of semiconductors, detect superconductivity, colossal magnetoresistance, and elucidate the mechanism for scattering of charge carriers in a wide variety of materials.<sup>7</sup>

By making electrical contact to a sample with a dissimilar metal, a voltage drop is produced (as in a thermocouple). If the contact resistance associated with this voltage drop is small compared to the resistance of the sample under study, one may use a two-probe method. A constant current is supplied and the voltage is measured across the same two leads.

On the other hand, when the resistance of the sample is of the same order of magnitude as the contact resistance, four probe methods are needed. In this method, four contacts are

made to each sample. Current is supplied to two of the leads and the voltage is measured across the other two to obtain the resistance ( $R=V/I$ ). In order to calculate the resistivity ( $\rho$ ), however, one may arrange the four contacts at the periphery of the sample, in a van der Pauw arrangement<sup>8</sup> (Fig. 1 shows one example) to simplify the determination of resistivity.

In such a configuration, van der Pauw showed that the resistivity can be determined simply as

$$\rho = \frac{\pi d}{\ln 2} R_{MN,OP}, \quad (1)$$

where  $d$  is the thickness of the cylindrical sample and the resistance is  $R_{MN,OP}=(V_P-V_O)/i_{MN}$ . The special arrangement of Fig. 1 is an example of one in which the sample possesses a line of symmetry;  $M$  and  $O$  are placed on a line of symmetry, while  $N$  and  $P$  are disposed symmetrically with respect to this line. In this case a single measurement suffices.

This manuscript describes an apparatus (approximately \$67,000 U.S.) that provides a simple and efficient means to measure the resistivity, in a van der Pauw arrangement, of combinatorial thin-film libraries.

<sup>a)</sup>Electronic mail: Kevin.Hewitt@Dal.ca; URL: <http://fizz.phys.dal.ca/~hewitt>

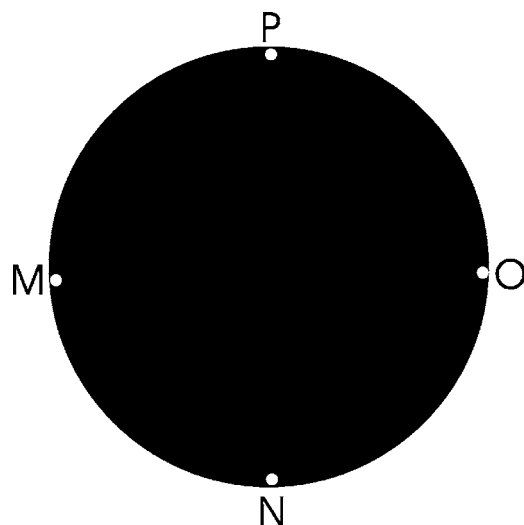


FIG. 1. van der Pauw arrangement of current and voltage leads on a cylindrical sample. A current is applied to contact *M* and grounded at *N*, and the voltage is measured across *O* and *P*.

## II. THE APPARATUS

The system consists of a vacuum chamber, ARS-830 closed-cycle helium compressor, Lakeshore 340 temperature controller, Keithley 2750 switch scanner, Varian Turbo-V 150 pump (969-9369), custom 196-pin device for electrical contact, and a custom-built liquid-nitrogen radiation shield.

### A. Cryostat and sample stage

The cryostat contains a 35 cm long copper cold finger. Heat is extracted from the cold finger by gaseous helium, which a compressor cycles through an expander operating on the principle of the Gifford-McMahon refrigeration cycle. The system has a cooling capability of 9 W at 20 K, and 3.5 W at 10 K. At the top of the cold finger is a copper sample stage, onto which is mounted the substrate with sputtered thin-film library (Fig. 2).

The sample stage consists of a 4 in.  $\times$  4 in.  $\times$  0.125 in. copper plate, having two recesses (0.05 in. in depth) machined at 90° relative to one another, to accommodate 3 in.  $\times$  3 in. or 4 in.  $\times$  4 in. square substrates. A screw machined from copper is used to connect the sample stage to the cold finger of the cryostat. Copper is used as it has a very high thermal conductivity over the temperature range of interest.

Good thermal contact between the substrate and the sample stage is provided by using a thin layer of copper impregnated vacuum grease (Cryocon grease).

### B. Temperature measurement

Silicon diode sensors (DT-470-SD-12) are placed at two points on the substrate, shown in Fig. 2. A Lakeshore 340 temperature controller monitors the output voltage, which is converted to the corresponding temperature with the DT-470 standard curve, for each sensor. The reported temperature has an accuracy of  $\pm 27$  mK at 4.2 K,  $\pm 110$  mK at 77 K, and  $\pm 85$  mK at 300 K, and precision of  $\pm 0.8$  mK at 4.2 K,  $\pm 11$  mK at 77 K, and  $\pm 8.4$  mK at 300 K.



FIG. 2. A quartz substrate with sputtered silver library loaded into the cryostat for measurement. Thermocouples can be seen fastened to the substrate via bolts.

In addition to the errors described above, one must consider the error associated with the placement of each sensor and whether its reading corresponds to the temperature of the library member whose resistance is being measured simultaneously. To minimize this error, the system is slowly cooled or warmed to reduce temperature variation across the library. In addition, libraries are deposited on alumina whose thermal conductivity ( $25.08 \text{ W m}^{-1} \text{ K}^{-1}$  at room temperature) is larger than quartz ( $3 \text{ W m}^{-1} \text{ K}^{-1}$  at 20 °C) or glass ( $1 \text{ W m}^{-1} \text{ K}^{-1}$ ) over the temperature range of interest. Good thermal conductivity ensures better uniformity in the temperature across the substrate, and hence the uncertainty in the measured sample temperature decreases.

The results presented here are completed with a warming rate of 0.3 K/min (i.e., 14.5 h over the temperature range 27–300 K). If there is a large variation in temperature it will be evident as a curvature in the resistivity versus temperature data for the silver library. The temperature-dependent resistivity data shown later is linear over the temperature range of the system, and hence this error is relatively small.

### C. Electrical contacts

After the substrate is loaded into the cryostat, the 196-pin device, seen in Fig. 3, is bolted onto it. The 196 pins precisely fit onto the 49-sample library for four-contact resistance measurements via the van der Pauw method. The pins have a spacing of 4.64 mm.

Electrical contact is made to the sample with spring-loaded pins (probes), having a gold-plated barrel with a rounded tip (Interconnect Devices Inc. S-2-D-4-G) (Fig. 3). The barrels have an outer diameter of 0.050 in. (1.27 mm), and terminate in a rounded tip onto the sample.

Springs made of a BeCu alloy supply a maximum force of 1.1 N (4.0 oz.), and provide for a travel of 0.1 in. (2.54 mm). The plunger for the spring is made of a gold-plated BeCu alloy.

The probes are inserted into a receptacle that is embedded in a 4.2 in.  $\times$  4.2 in.  $\times$  0.4 in. material FR4, a woven fine

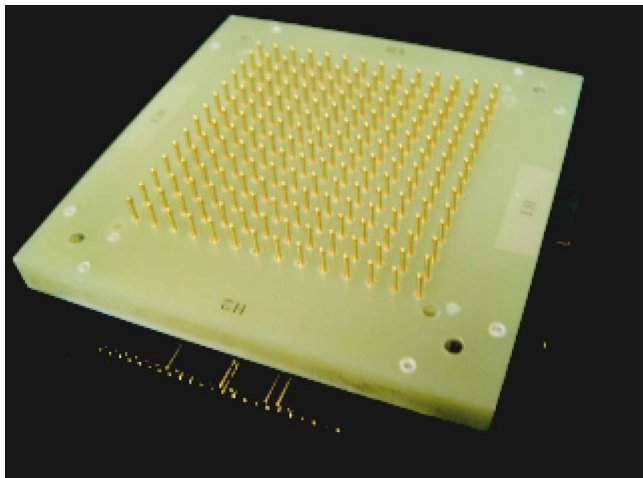


FIG. 3. The 196-pin device which makes electrical contact to the 49-sample thin-film library for four-contact resistivity measurements. The shortest distance between pins is 4.64 mm.

glass epoxy (G10) laminate (fiberglass hot-pressed together with glass-filled epoxy resin). This material has a thermal conductivity of 3 W/mK (comparable to window glass) and a thermal expansion coefficient of  $10\text{--}13 \times 10^{-6} \text{ K}^{-1}$  (comparable to steel). Wire wrap terminations allow connection of the probes to four 50-pin headers that are firmly attached to the pin device. 50-conductor ribbon cable (Nu Data, Mini-D50, 1/2 pitch) are attached to each of the four headers. These are passed outside the cryostat through four 50-pin feedthrough ports, hermetically sealed. Thermal grounding of the ribbon cables is achieved by securing them to the first and second stage of the cold finger.

#### D. Voltage and current controls

A Keithley 2750 switch scanner measures the potential difference across each member of the library when a current (30 mA for the THIN library and 100 mA for the THICK library) is supplied using a Lakeshore 120 constant current source. Each channel is scanned every 17 s.

Three four-wire mode, 40-channel differential multiplex units (Keithley 7708) are used to connect the output leads to the Keithley 2750. For each multiplex unit, 80 two-wire channels are available, hence in the current system three units are used. Up to one additional multiplex port is available on the Keithley unit. As such, up to 320 channels or an 80-member library, could potentially be measured with the system.

#### E. Reducing electrical noise

To reduce electrical noise, caused by changing current in one wire inducing current in another, or the same, the wires leaving the cryostat are twisted, separately, into pairs corresponding to the voltage or current leads for one sample in the library.

In addition, the original heater (Kapton Foil heater) was replaced with a twisted pair of 32 AWG Nichrome wire (four twists per inch) cut to a length that produced a resistance of 50  $\Omega$ . By twisting the pair, the net field produced by the wires is effectively zero.

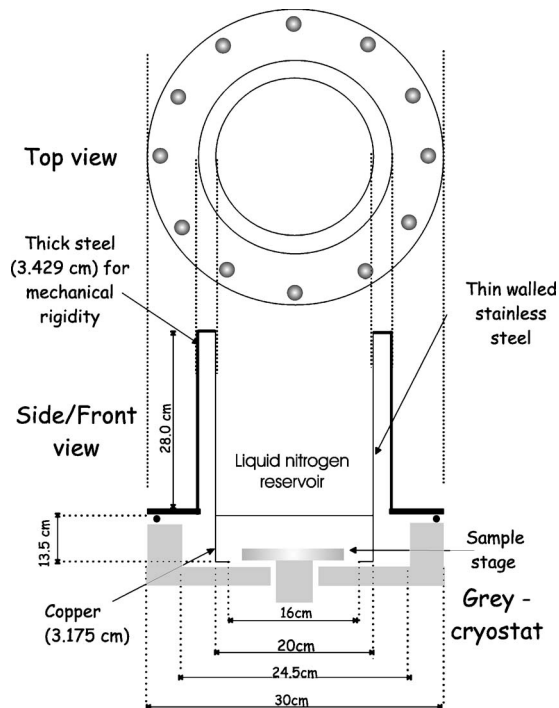


FIG. 4. A schematic drawing of the radiation shield. The shield rests on, and makes a vacuum seal to, the cryostat with the aid of an O-ring.

The helium lines to/from the compressor and expander are buried in sand to dampen vibration from the compressor.

#### F. Thermal radiation effects

A 500 l/s turbo vacuum pump evacuates the cryostat to typically 20  $\mu\text{Torr}$  before cryopumping of water vapor reduces the pressure at low temperature. This vacuum minimizes conductive heat load to the cold finger.

The pin device, large sample stage, and ribbon cables together present a significant thermal load for the system. Without having the pin device in the system, temperatures of 6 K at the cold finger were achieved. When the pin device was inserted, the system could not achieve stable temperatures below 37 K. As the temperature approached this value from above, the temperature rose to near 60 K and then fell back to 37 K, repeating several times. These changes were accompanied by corresponding changes in the system pressure as measured by a thermocouple gauge (VRC 912086 021118002).

Since the vacuum is at least 20  $\mu\text{Torr}$  at the turbo, it was felt that thermal radiation was causing this effect, as the system was not initially provided with a radiation shield. Radiative heating on the area (362  $\text{cm}^2$ ) of the pin device and sample stage produces a thermal load of 9.0 W at 38 K, when the sample stage and pin device are surrounded by the cryostat walls at 296 K. Thus the refrigerator cannot remove heat at a sufficient rate to offset radiative heating. Consequently, one must introduce a radiation shield in order to effectively reduce radiative heating.

A liquid-nitrogen radiation shield was designed, as shown in Figs. 4 and 5. Liquid nitrogen fills a Dewar, to which is vacuum welded a copper cylinder whose diameter is large enough to fit over the entire pin device and sample

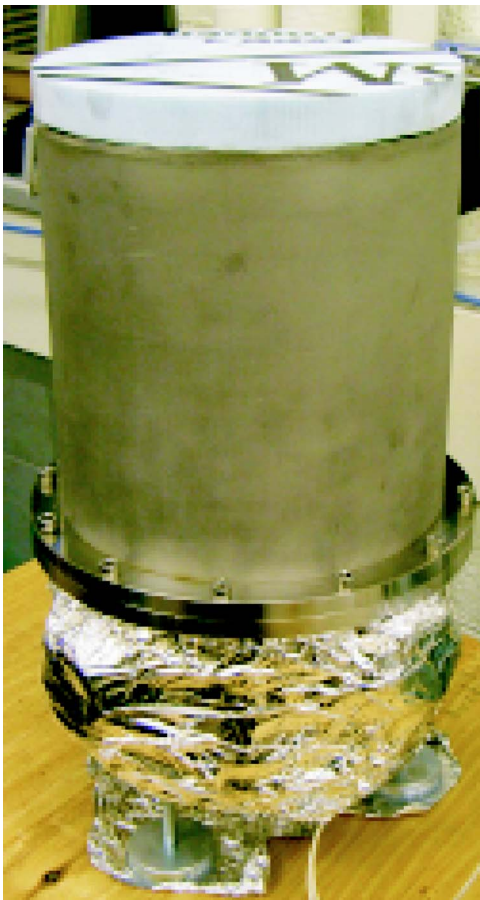


FIG. 5. The radiation shield installed on the cryostat. Liquid nitrogen is filled at the top (after the styrofoam top is removed). The vacuum chamber containing the samples can be seen near the bottom of the picture.

stage. The walls of the Dewar are made of thin stainless steel to reduce heat transfer by conduction. A vacuum space exists between the inner concentric stainless-steel cylinder (20 cm diam) containing the Dewar of liquid nitrogen and the outer concentric cylinder of 3.4 mm thick stainless steel (25.4 cm diam) used for structural support. As such, heat transfer by conduction is minimized. With this radiation shield in place, a minimum temperature of 27 K was achieved on the library substrate, and 7 K at the cold finger!

### G. Geometric errors

The resistivity is given by Eq. (1) when the contacts are sufficiently small, and situated at the periphery of the sample disk (Fig. 1). van der Pauw determined the relative error ( $\Delta\rho/\rho$ ) in the calculated value of the resistivity for a circular disk of diameter  $D$ , on which one contact is nonideal. That is, consider a circular disk of radius  $D$  with the contacts mutually  $90^\circ$  apart, as in Fig. 1. If one of the contacts, although a point, is situated at a distance  $l$  from the periphery, the relative error is

$$\frac{\Delta\rho}{\rho} = \frac{-l^2}{2D^2 \ln 2}. \quad (2)$$

The circular sample disks in the library are 8.00 mm in diameter, while the shortest distance between pins is 4.64 mm. Thus, the diagonal distance is 6.57 mm between pins, lead-

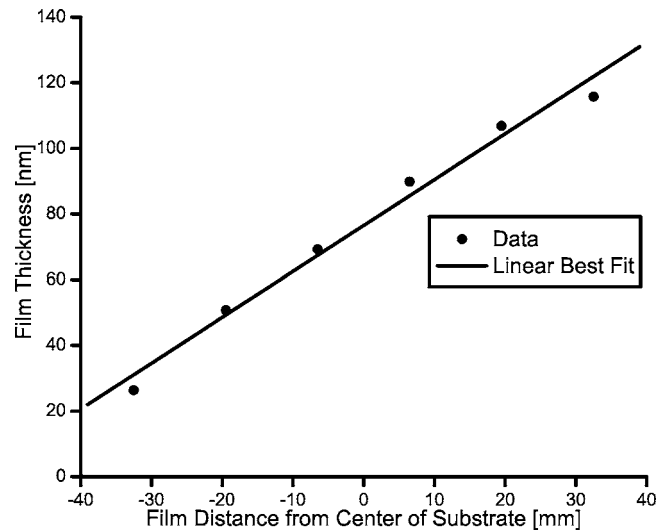


FIG. 6. Silver film thickness vs distance from the center of the substrate (opposite target center) for the THIN library. Slope=1.40 nm/mm.

ing to an offset  $l=0.72$  from the edge of the sample. As a result, the geometrical error is 0.6% per lead or 2.4% for the four leads taken together.

The resistivity of silver is less than any other element (except a superconductor below  $T_c$ , where resistivity vanishes). Hence the voltage drop will be smallest for silver and will therefore place a lower limit on the signal-to-noise ratio of the apparatus. Thus, if the system were shown to measure the resistance of silver as a function of temperature well, it would be capable of measuring the resistance trends of any good conductor or superconductor. Thus silver films were chosen as the first test case.

### III. LIBRARY PREPARATION

Thin films have been deposited using a Corona Vacuum Coaters (Vancouver, BC, Canada) magnetron sputtering system. Films were deposited onto a rotating table on which various substrates are placed. Two inch diameter targets with a thickness of 1/4 in. or 1/8 in. are mounted in a magnetron containing water-cooled, Nd-Fe-B magnets (Tridus Corporation, Rancho Dominguez, CA, USA). Vacuum levels of  $10^{-7}$  Torr are achieved using a 500 l/s turbo pump, in conjunction with a Polycold cryopump, which removes water vapor by condensation onto its coils, which are cooled to  $-160^\circ\text{C}$  by a proprietary non-chlorofluorocarbon (CFC) refrigerant.

The dc magnetron sputtering of the silver target (Pure-Tech, 99.99%,  $\rho=1.59 \mu\Omega\text{ cm}$ ) was completed with a chamber pressure of 3.81 mTorr (0.5 Pa) and 2 sccm Ar gas in the chamber. A potential of 310 V was used to produce a power of 50 W dc, and the films were deposited over 30 min for the THIN library and 170 min for the THICK library. All sputtered samples were stored in an argon atmosphere to prevent oxidation until used for almost all measurements.

The library is deposited onto alumina substrates (10.16 cm  $\times$  10.16 cm, PiKem, Shropshire, UK), which were subjected to the following cleaning procedure. They are cleaned with acetone, methanol, and a Kimwipe, then placed

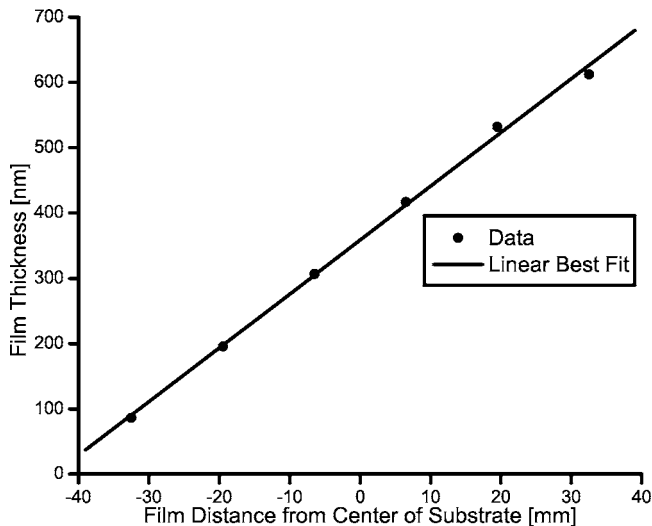


FIG. 7. Silver film thickness vs distance from the center of the substrate (opposite target center) for the THICK library. Slope=8.2 nm/mm.

in the “pumpkin” overnight. The pumpkin is a container of ethanol very near its boiling point above which the substrates are mounted. The ethanol constantly evaporates and condenses, adsorbing onto the substrates. Ethanol liquid gradually drips off the substrates back into the bath at the bottom of the pumpkin. In this manner dirt is removed from the substrates as the ethanol condenses then drips off. More pure ethanol then evaporates onto the substrates and the cycle repeats. Alumina substrates were used since they are insulating, inexpensive, and can be heated to high temperatures (mp 2072 °C), and typically provide better adhesion than glasses.

The alumina substrates had an aluminum shadow mask taped to them in the 7×7 grid pattern. Three substrates are placed on the same sputtering table such that their centers were in the center of the sputtering track (the area of the table that has material sputtered on it).

When the silver targets are sputtered, a deposit that varies linearly is obtained using an appropriately designed mask placed between the target and substrate.<sup>9</sup> Thicknesses are deduced by depositing the film onto 1.3 cm diam preweighed aluminum disks (secured to the table with double-sided tape) whose mass is measured with a Cahn 29 electrobalance. Using the bulk density of silver (10.50 g/cm<sup>3</sup>), the thickness is estimated as  $t=4m/\pi d^2\rho$ . The change in thickness across the library is shown in Fig. 6 for a THIN library (48–123 nm) (Ref. 10) and Fig. 7 for a THICK library (106–639 nm).

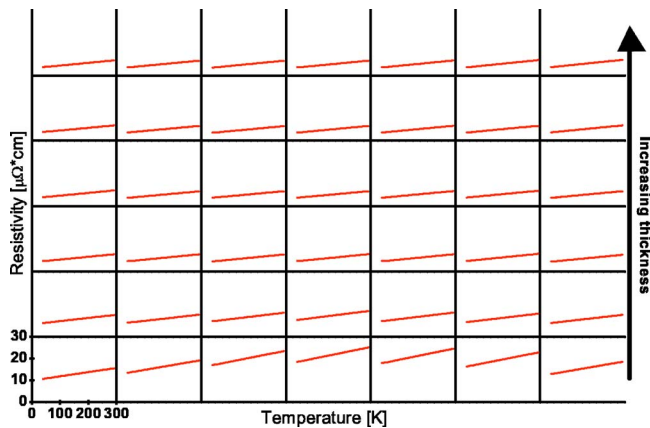


FIG. 8. Resistivity vs temperature data for silver thin films on warming: THIN library (48–123 nm). The top row are the thickest films and hence the least resistive. The film thickness linearly increases with each row, to the thinnest film in the bottom row. Horizontal axis ranges from 0 to 300 K and the vertical axis ranges from 0 to 30 μΩ cm.

There were three sets of disks on the sputtering table. The thickness data are an average of all three sets.

#### IV. RESULTS

The temperature dependence of electrical resistivity of the THIN silver (48–123 nm) library on warming can be seen in Fig. 8. The minimum temperature achieved at the samples was 38 K and the maximum was room temperature.

The thickest films are in the top row, row 1, and the thinnest are in the bottom row, row 6, where the in-row variation in thickness is most significant compared to the mean thickness. The thickness of sputtered silver is equal along a given radial direction from the center of the sputtering machine and the samples are sputtered in a 7×7 film square. Hence, within a row of films the outermost films will be slightly thicker and less resistive. This trend can be seen in row 6. Since the films are not equal thickness, a conversion from the electrical resistance to the intrinsic resistivity was made using Eq. (1) so a comparison of all films could be made. By simply measuring the distance from the center of the sputtering table to the center of the substrates (135 mm) and knowing the shortest distance between the center of adjacent members of the library to be 10.15 mm, the distance from the center of the sputtering table was calculated for each member of the library. Using the thickness best-fit line of Fig. 6, the thickness of each film was calculated and is

TABLE I. Average thickness (nm) for each member of the THIN (48–123 nm) film library. Row 1 was the furthest from the center of the sputtering table so is the thickest. Row 6 is the thinnest row as it was closest to the center of the sputtering table. The variation in each thickness is ±7 nm.

(i, j)	Column 1	Column 2	Column 3	Column 4	Column 5	Column 6	Column 7
Row 1	123	121	120	119	120	121	123
Row 2	109	107	106	105	106	107	109
Row 3	95	93	91	91	91	93	95
Row 4	81	79	77	77	77	79	81
Row 5	67	65	63	62	63	5	67
Row 6	54	51	49	48	49	51	54

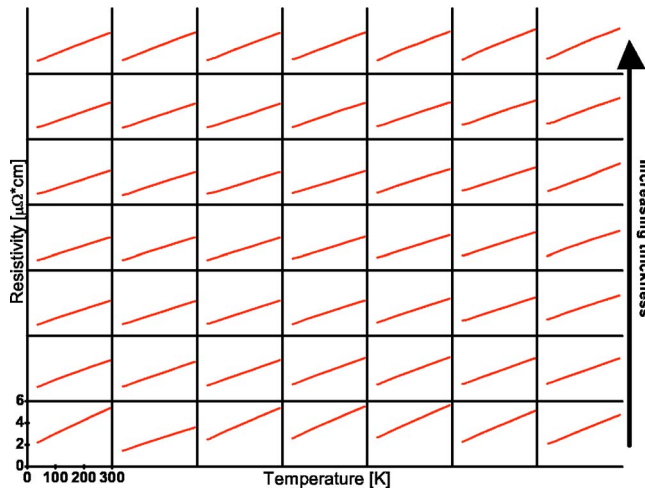


FIG. 9. Resistivity vs temperature data for silver thin films on warming: THICK library (106–639 nm). The top row are the thickest films and hence the least resistive. The film thickness linearly increases with each row, to the thinnest film in the bottom row. Horizontal axis ranges from 0 to 300 K and the vertical axis ranges from 0 to 6  $\mu\Omega$  cm.

reported in Table I. The thicknesses of the library members were calculated to be the same in column 5 as column 3 and column 6 as column 2 and column 7 as column 1, which is expected since the grid of films is symmetric about the central column, column 4.

The variation of the film thickness is quite large due to the increase of thickness over the substrate. The rate of increase of film thickness is the slope of Fig. 6, namely, 1.40 nm/mm, that is, a 1.40 nm increase in thickness for every 1 mm traversed on the substrate (in the direction of increasing thickness). Since every member of the library is 8.00 mm in diameter, the variation across each one is 11.2 nm. The variation in film thickness for each member is thus  $\pm 6$  nm. The uncertainty in the thickness is mainly due to the fact that the films were assumed to have bulk Ag density. Further uncertainty is due to the scale used to weigh the disks. Hence, the total variation and uncertainty in the film thickness is about  $\pm 7$  nm. This is very significant compared to the thickness of the films, particularly for the thinner films.

The resistivity and thickness of the samples in the THICK library are described in Figs. 7 and 9 and Table II. These measurements were completed under identical conditions except that the current used for the THIN library was 30 mA while 100 mA was used for the THICK library.

TABLE II. Average thickness (nm) for each member of the THICK (106–639 nm) film library. The variation in each thickness is  $\pm 35$  nm.

$(i, j)$	Column 1	Column 2	Column 3	Column 4	Column 5	Column 6	Column 7
Row 1	639	623	614	611	614	623	639
Row 2	557	540	530	527	530	540	557
Row 3	475	457	446	442	446	457	475
Row 4	394	375	362	358	362	375	394
Row 5	314	292	279	274	279	292	314
Row 6	234	210	195	190	195	210	234
Row 7	156	129	112	106	112	129	156

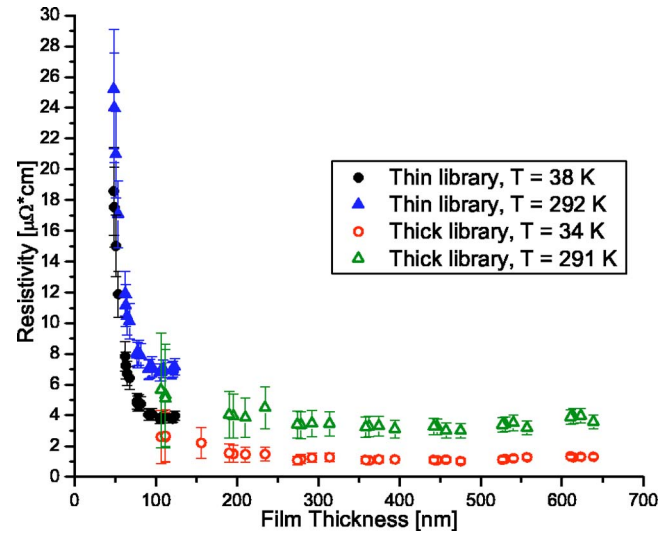


FIG. 10. The resistivity vs film thickness for both thick and thin silver libraries.

When combined, the resistivity as a function of thickness is obtained over a large range (48–639 nm) in two experiments! The data are plotted in Fig. 10.

The slope of all  $\rho(T)$  plots in Figs. 8 and 9 were taken from linear best fits to the data. Figure 11 shows this slope, known as the temperature coefficient of resistivity, as a function of film thickness. The well-known<sup>11</sup> coefficient for pure silver is 0.0061  $\mu\Omega$  cm  $K^{-1}$ .

## V. DISCUSSION

### A. Resistivity

The electrical resistivity of most metals is dominated at room temperature by collisions of the conduction electrons with lattice vibrations and at low temperatures by collisions with impurity atoms and mechanical imperfections of the lattice. For dilute impurities or defects, Matthiessen's empirical rule divides these effects into a temperature-dependent ( $\rho_L$ ) and temperature-independent part ( $\rho_i$ ), respectively.<sup>7</sup> That is, impurity or defect scattering provides a positive offset to the resistivity data.

Meaden<sup>11</sup> reports an intrinsic value for the resistivity of bulk silver as 1.588  $\mu\Omega$  cm at 291 K (corrected for impurity scattering). The present results give an average resistivity of  $3.4 \pm 0.5$   $\mu\Omega$  cm for films thicker than 300 nm. It is important to determine whether the difference is an instrumental

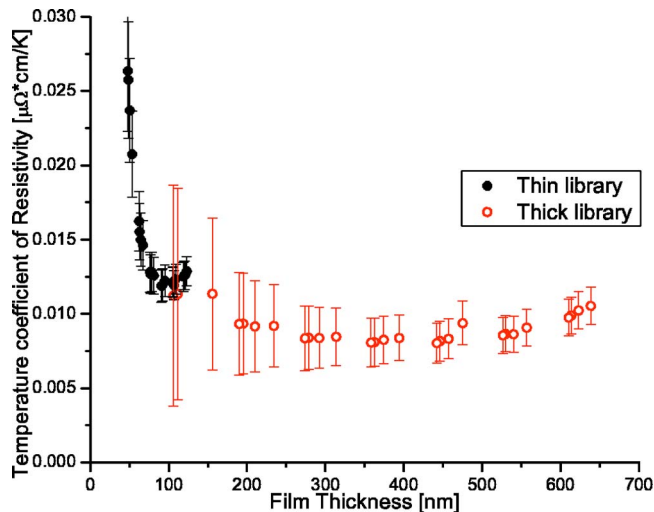


FIG. 11. The temperature coefficient of resistivity as a function of thickness.

error or one derived from the characteristics of the films. To reconcile the difference, one needs to consider the effect of atomic impurities or vacancies.

Electron dispersive spectroscopy (EDS) measurements reveal that the films have a purity of 99%. However, since EDS measurements are only accurate to within 1%, there is not much one can deduce from such a measurement. It is possible, however, to compare the results to those obtained by Maréchal *et al.*<sup>12</sup> who explored the argon pressure dependence of the electrical resistivity of 200 and 700 nm thick films prepared by rf magnetron sputtering of silver onto silicon and glass substrates at 180 °C. They found a grain size of approximately 80 nm and a contraction of the lattice by 0.12%–0.20% and 0.05%–0.12% for films prepared under an argon pressure of 0.2 and 1.0 Pa, respectively. Their films exhibit a resistivity of 1.5–2.0  $\mu\Omega$  cm. The data presented in this manuscript is derived from films deposited by dc magnetron sputtering at an argon pressure of 0.5 Pa onto alumina substrates affixed to a water-cooled table. First, as the deposition temperature used in the present work is lower than that of Maréchal *et al.*,<sup>12</sup> one would expect more defects as the silver atoms will experience a higher quenching rate. Sec-

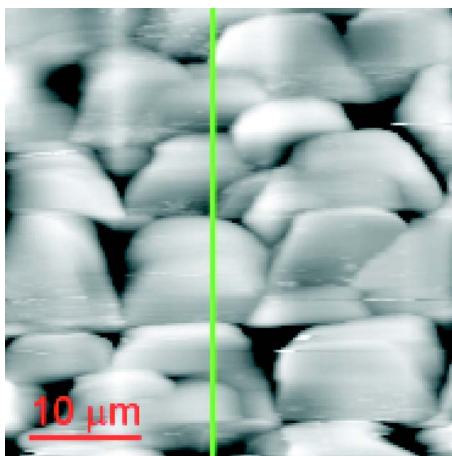


FIG. 12. AFM image, looking downward, for the 123 nm Ag film. The vertical line is the location that the cross section was taken for Fig. 13.

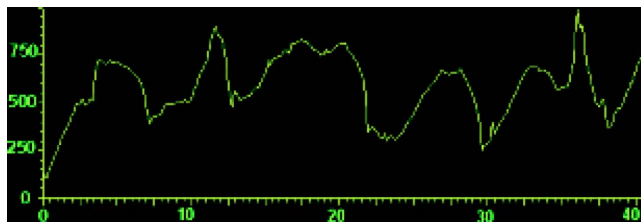


FIG. 13. The cross section, showing height vs distance, traverses along the vertical line in Fig. 12. The zero distance corresponds to the bottom of Fig. 12. Vertical scale is nm and horizontal scale is  $\mu\text{m}$ .

ond, the energy and flux of argon ions are relatively higher in rf than in dc discharge, all other things being equal.<sup>12</sup> As the energy and flux of the argon ions increases, the density of sputter-deposited films increase.<sup>13</sup> Thus, all other things being constant, films sputtered by dc magnetron sputtering will have a smaller density than those sputtered by rf techniques. Consequently, one expects the defect density to be larger for films produced with higher quenching rates and lower argon ion flux and energy. Thus it is expected that the scattering rate by vacancies, defects would be greater in the films deposited by dc magnetron sputtering onto water-cooled substrates, as found in this work. In fact, the resistivity data presented here are consistent with those of Maréchal *et al.*<sup>12</sup> for an argon pressure of 6 Pa, as one would expect since higher-pressure rf magnetron sputtering would effectively decrease the energy of argon ions, mimicking the effect of dc sputtering. Moreover, for many materials an impurity in solid solution creates a residual resistivity of 1  $\mu\Omega$  cm per atomic percent impurity.<sup>7</sup> A vacancy or defect concentration of approximately 1%–2% is therefore entirely consistent with the resistivity and EDS data.

Below approximately 100 nm, the resistivity of the films increase dramatically. Two effects must be considered in this regard. First, the substrate is very rough (300–500 nm) as deduced from atomic force microscope (AFM) images (Figs. 12 and 13). The film is characterized by  $\approx 10 \mu\text{m}$  islands, which reflect the topography of the underlying substrate as seen in separate AFM measurements. On one of these islands one observes (Figs. 14 and 15) that the film has a surface roughness of approximately 8–10 Å, or 2–3 atomic layers

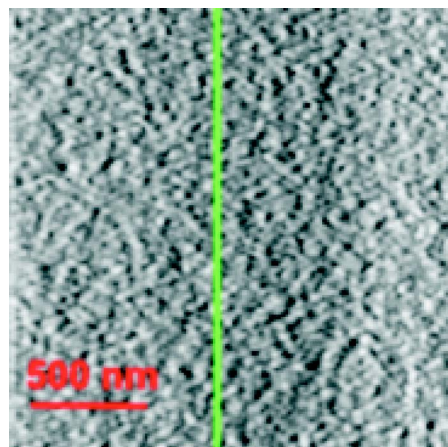


FIG. 14. High magnification AFM image, looking downward, near the center of the 123 nm thick Ag film.

over 2000 nm. For silver, the Fermi wave vector ( $k_F$ ) is  $1.20 \times 10^8 \text{ cm}^{-1}$ , which corresponds to a wavelength of  $\lambda_F = 2\pi/k_F = 523 \text{ \AA}$ . Thus the wavelength is large compared with the surface roughness on an island, and the reflections are specular. At the boundary of these islands the film may be discontinuous for the THIN library. Hence boundary scattering effects will certainly increase the resistivity.

Second, on steep edges of the substrate the film will be very thin and as such, surface scattering effects become important. The thickness dependence of resistivity in the surface scattering regime is described by Ziman.<sup>14</sup> If the mean free path ( $\Lambda_o$ ) of itinerant electrons is large compared with the thickness ( $t$ )  $\rho/\rho_o \approx 4\Lambda_o/3t \ln(\Lambda_o/t)$ , while if  $\Lambda_o \ll t$ , then  $\rho/\rho_o \approx (1 - 3\Lambda_o/8t)^{-1}$ . A least squares fit using either function could not account for the data, and this is most likely due to the fact that there is a large distribution of thicknesses for the rough alumina substrate. However, one cannot rule out these effects. As a consequence, both boundary and surface scattering effects may contribute to the enhanced resistivity. Further experiments are required to disentangle these effects.

## B. Temperature coefficient of resistivity

The well-known<sup>11</sup> temperature coefficient of resistivity for pure silver is  $0.0061 \mu\Omega \text{ cm K}^{-1}$ . The data for most of the thicker films is consistent with this result within experimental error. However, at thicknesses less than 100 nm the temperature coefficient of resistivity (Fig. 11) is clearly larger.

A change in the temperature coefficient of resistivity may be due to a change in the lattice constant, elastic properties or electronic structure of the solid. As the film thickness is reduced one would expect there to be significant changes in these parameters. In fact, Eberle *et al.*<sup>18</sup> found in evaporated silver films that there is a strong decrease in the elastic constants below 100 nm, e.g., at a thickness of 34, 48, 61, and 82 nm, the value of  $c_{44} = 6, 14, 20$  (estimate), and 21 (estimate) GPa. The bulk value is known<sup>20</sup> to be 46 GPa. Thus there is a decrease in the elastic constant  $c_{44}$  by a factor of about 8. The relationship between the Debye temperature ( $\Theta_D$ ) and the elastic constants in a cubic system has been derived semiempirically by Blackman<sup>19</sup> as

$$\Theta_D^3 = \frac{3.15}{8\pi} (h/k)^3 \frac{s}{\rho^{3/2} v_a} (c_{11} - c_{12})^{1/2} (c_{11} + c_{12} + 2c_{44})^{1/2} (c_{44})^{1/2}, \quad (3)$$

where  $h$  is Planck's constant,  $k$  is Boltzmann's constant,  $s$  is the number of atoms in the unit cell,  $v_a$  is the unit cell volume, and  $\rho$  is the density. Using the bulk values of the elastic constants from Kittel<sup>7</sup> for Ag and those from Eberle<sup>18</sup> for thin Ag films (at a thickness of 34 nm,  $c_{44} = 6$  GPa,  $c_{11} = 120$  GPa), and assuming no change in  $c_{12}$  and the density of the film from bulk values results in a decrease of the Debye temperature by a factor of 2/3. Formal transport theory for electronic conduction in metals predict that the temperature-dependent part of the resistivity ( $\rho_L$ ) is inversely proportional to the Debye temperature ( $\rho_L \sim T/\Theta_D \rho_\Theta$ ) for  $T \gg \Theta_D$  and is inversely proportional to the fifth power of the

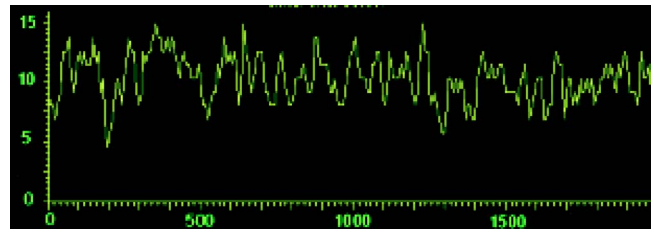


FIG. 15. Cross section along the vertical line in Fig. 14. Location of this film is approximately at the center of the thickest film. Vertical scale is  $\text{\AA}$  and the horizontal scale is nm.

Debye temperature [ $\rho_L \sim 497.6(T/\Theta_D)^5 \rho_\Theta$ ] for  $T \ll \Theta_D$ . The Debye temperature for bulk silver is 225 K.<sup>7</sup> It is evident from Figs. 8 and 9 that the resistivity is linear in  $T$ . Thus one expects the temperature coefficient of resistivity to be inversely proportional to  $\Theta_D$ , leading to an increase in the slope by a factor of 1.5. Figure 11 shows there is a corresponding increase in the temperature coefficient of resistivity, to  $0.026 \mu\Omega \text{ cm/K}$ , whereas the bulk value<sup>11</sup> is  $0.0061 \mu\Omega \text{ cm K}^{-1}$ , i.e., a factor of 4 increase. Thus the observed changes in the temperature coefficient of resistivity are not fully accounted for by changes in the Debye temperature.

If grain-boundary scattering is the dominant mechanism, there should be no change in the temperature-dependent part of the resistivity. This was found by de Vries,<sup>15</sup> who studied the temperature and thickness dependence of evaporated thin films of silver on  $\text{SiO}_2/\text{Si}$  substrates. It was found that the temperature coefficient of resistivity was independent of thickness and equal to the bulk value, for thicknesses of 23, 34, 48, 102, and 300 nm. This is clearly not the result seen in this work.

If, on the other hand, surface scattering is the dominant mechanism, then the temperature-dependent part of the resistivity will vary with thickness, as found by Sambles *et al.*<sup>16</sup> for large grained thin films of gold (Fig. 9 in their paper, thickness = 95, 277, and 590 nm). Given the roughness of the substrate (Fig. 13) and the fact that the steeply sloping sides are sparsely covered, one expects the film to be very thin along these slopes. Thus surface scattering will play a role in altering the temperature dependence. An intuitive reason for this is outlined by de Vries.<sup>17</sup> Only electrons within a distance of less than the mean free path ( $\Lambda_o$ ) from the surface can be scattered at the surface. Since  $\Lambda_o$  depends on the temperature, surface scattering tends to affect the temperature-dependent part of  $\rho$ . Moreover, in very thin regions conduction will be governed by thermally activated hopping, which will introduce an additional temperature dependence.

## ACKNOWLEDGMENTS

The financial support of the Natural Sciences and Engineering Research Council of Canada is gratefully acknowledged. M. H. Jericho provided invaluable input into all aspects of the project, and his contribution is greatly appreciated. Valuable discussions with J. R. Dahn and T. Monchesky were very helpful. The authors thank A. Touhami for his assistance in obtaining the AFM images.

- <sup>1</sup>K. Kennedy, T. Stefansky, G. Davy, V. F. Zackay, and E. R. Parker, *J. Appl. Phys.* **36**, 3808 (1965).
- <sup>2</sup>J. J. Hanak, *J. Mater. Sci.* **5**, 964 (1970).
- <sup>3</sup>X. D. Xiang, X. Sun, G. Briceno, Y. Lou, K-A. Wang, H. Chang, W. Wallace-Freedman, S-W. Chen, and P. Schultz, *Science* **268**, 1738 (1995).
- <sup>4</sup>R. B. van Dover, L. F. Schneemeyer, R. M. Fleming, *Nature (London)* **162**, 392 (1998).
- <sup>5</sup>H. Chang, I. Takeuchi, and X.-D. Xiang, *Appl. Phys. Lett.* **74**, 1165 (1999).
- <sup>6</sup>X.-D. Xiang, *Annu. Rev. Mater. Sci.* **29**, 149 (1999).
- <sup>7</sup>C. Kittel, *Introduction to Solid State Physics*, 7th ed. (Wiley, New York, 1996).
- <sup>8</sup>L. J. van der Pauw, *Philips Tech. Rev.* **20**, 220 (1958).
- <sup>9</sup>J. R. Dahn, S. Trussler, T. D. Hatchard, A. Bonakdarpour, J. R. Mueller-Neuhaus, K. C. Hewitt, and M. Flischauer, *Chem. Mater.* **14**, 3519 (2002).
- <sup>10</sup>In the thinnest row of silver films there was significant shadowing from the aluminum mask, and the film itself was not continuous. This thinnest row in the THIN silver films is therefore excluded from all analysis hereon since the films are not representative of intrinsic silver.
- <sup>11</sup>G. T. Meaden, *Electrical Resistance of Metals* (Plenum, New York, 1965).
- <sup>12</sup>N. Maréchal, E. Quesnel, and Y. Pauleau, *J. Vac. Sci. Technol. A* **12**, 707 (1994).
- <sup>13</sup>K-H. Müller, *J. Appl. Phys.* **62**, 1796 (1987).
- <sup>14</sup>J. M. Ziman, *Electrons and Phonons: The Theory of Transport Phenomena in Solids* (Clarendon, Oxford, 1972).
- <sup>15</sup>J. W. C. de Vries, *Thin Solid Films* **167**, 25 (1988).
- <sup>16</sup>J. R. Sambles, K. C. Elsom, and D. J. Davis, *Philos. Trans. R. Soc. London, Ser. A*, **304**, 365 (1982); J. R. Sambles, *Thin Solid Films* **106**, 321 (1983).
- <sup>17</sup>J. W. C. de Vries, *J. Phys. F: Met. Phys.* **17**, 2403 (1987).
- <sup>18</sup>R. Eberle, T. Kresser, and M. Pietralla, *Thin Solid Films* **408**, 169 (2002).
- <sup>19</sup>M. Blackman, *Philos. Mag.* **42**, 1441 (1951).
- <sup>20</sup>O. L. Anderson, in *Physical Acoustics, Principles and Methods*, edited by W. P. Mason and R. N. Thurston (Academic, New York, 1964), Vol. 3b, p. 77.

Review of Scientific Instruments is copyrighted by the American Institute of Physics (AIP). Redistribution of journal material is subject to the AIP online journal license and/or AIP copyright. For more information, see <http://ojps.aip.org/rsio/rsicr.jsp>